Cohesion and polymorphism in solid rubidium chloride

2006 J. Phys.: Condens. Matter 18 683

(http://iopscience.iop.org/0953-8984/18/2/023)

INSTITUTE OF PHYSICS PUBLISHING JOURNAL OF PHYSICS: CONDENSED MATTER

J. Phys.: Condens. Matter **18** (2006) 683–702 doi:10.1088/0953-8984/18/2/023

Cohesion and polymorphism in solid rubidium chloride

N C Pyper[1], A I Kirkland[2] and J H Harding[3]

[1] University Chemical Laboratory, Lensfield Road, Cambridge CB2 1EW, UK
[2] Department of Materials, University of Oxford, Parks Road, Oxford OX1 3PH, UK
[3] Department of Engineering Materials, Sir Robert Hadfield Building, University of Sheffield, Mappin Street, Sheffield S1 3JD, UK

Received 15 July 2005
Published 16 December 2005
Online at stacks.iop.org/JPhysCM/18/683

Abstract

The cohesive energetics of three phases of solid cubic rubidium chloride, the zinc blende structured 4:4 phase, the 6:6 sodium chloride polymorph and the 8:8 phase with the cesium chloride structure, are computed using a non-empirical fully ionic model. The rearrangement energies needed to convert free anions to their optimal states in-crystal, two-body inter-ionic potentials, plus the further contributions arising from electron correlation, are reported. The 'optimal' anion–anion potentials, computed by using at each geometry the optimal wavefunction, are compared with the 'frozen' potential using the same wavefunction at all geometries.

The lattice energy of the 4:4 structure is predicted to be some 40 kJ mol^{-1} smaller than that of either the 6:6 or the 8:8 phases. Introduction of the Axilrod–Teller triple dipole dispersion interactions and the vibrational zero point energy predicts the 8:8 phase to lie 3.2 kJ mol^{-1} lower in energy than the 6:6 structure. This is both consistent with radius ratio arguments and supported by two separate experiments that strongly suggest that the 8:8 phase is favoured over the 6:6 structure at low temperatures even though the latter is more stable at ambient temperatures.

A shell model description is presented for the ion-induced dipole interactions that arise both in small clusters and in crystals encapsulated in nanotubes. The elastic constants and entropy at 300 K predicted for the 6:6 phase from this model by using the GULP program agree well with experiment. A smaller entropy is predicted for the 8:8 structure.

1. Motivation

Two broad classes of reason motivate the present theoretical study, using a fully ionic description, of three different cubic polymorphs of solid rubidium chloride. The assumption of full ionicity underlying these computations is justified by abundant experimental and theoretical

evidence, reviewed elsewhere [1, 2], that many crystals are essentially fully ionic. Two x-ray crystallographic studies of rubidium chloride are especially relevant here because the electron density distributions measured [3, 4] were entirely consistent with fully ionic bonding with no evidence for any covalency.

The first broad reason for studying rubidium chloride is that the cohesive properties of the different cubic phases, and the inter-ionic interactions through which these are determined, constitute one of the most interesting extensions of previous theoretical investigations of such properties of polar solids [5–12]. In particular, the difference between the cohesive energies of the six coordinated phases of alkali halides having the sodium chloride structure (the 6:6 structure) and the eight-fold coordinated phases having the cesium chloride structure (the 8:8 structure) proved, for many years, to be very hard to calculate. Thus theoretical studies, starting with Hund in 1925 [13] and extending over several decades through the 1937 work of May [14, 15], predicted incorrectly that the 6:6 phase of CsCl had a lower energy than the 8:8 structure observed to be the most stable at room and lower temperatures. This difficulty was, however, resolved by the observation [6, 12] that the expression for the cohesive energy of an ionic solid contains, in addition to the usual Madelung term, short range two-body inter-ionic repulsions and the dispersive attractions, the rearrangement energy needed to convert an isolated anion into its form optimally adapted to the crystal. The presence of the rearrangement energy showed that the two-body interactions in previous theories [13–16], which did not explicitly introduce the rearrangement energy, were actually effective potentials which included, in addition to the true two-body interactions, a structure-dependent fraction of the rearrangement energy. Two different lines of reasoning suggest that the explanation [6, 12] of why CsCl adopts the 8:8 structure at ambient temperatures might also apply to RbCl at low temperatures. In this event, the 8:8 structure would have a lower energy than the 6:6 phase with the latter being the stable phase at room temperature solely on account of its greater entropy. First, this possibility is suggested by the well known radius ratio rules [17–19], which although possibly somewhat uncertain in their theoretical foundation, can successfully rationalize a wide range of experimental data. These rules predict that an alkali halide will adopt the 8:8 structure only if the ratio of the cation to the anion radius is greater than 0.732. Interestingly, for RbCl this ratio is found to be 0.82 using the most standard (Pauling) radii [18] of 1.48 Å for Rb^+ and 1.81 Å for Cl^-; even larger ratios are predicted using radii [20–22] derived from electron density maps. Second, two studies of multi-layered deposits of RbCl, the substrate being first TlCl [23] and later amorphous bases [24], indicated that the 8:8 phase was indeed more stable than the 6:6 structure at low temperatures. The failure to generate the 8:8 phase either by cooling the 6:6 material from room temperature or by depositing it directly onto a glass capillary at low temperatures can be explained by postulating [23] that the crystal becomes kinetically trapped in the higher energy 6:6 phase in accordance with Ostwald's step rule [25, 26]. It is one object of this paper to investigate the relative energies of these two phases using the methods known to be successful for CsCl [6, 12].

The second broad class of reason motivating the study of inter-ionic forces is provided by recent investigations [27–31] of the structures of small nanocrystals encapsulated in carbon nanotubes. Newly developed methods in transmission electron microscopy [32, 33] at atomic resolution have enabled the structures of such encapsulated crystals to be determined. The structures differ from those of the corresponding bulk materials by at least changes in the cell dimensions and lowerings of symmetry [28, 31], and these may be accompanied by further distortions [27]. For some materials entirely novel structures not exhibited by the bulk are observed [34]. Our present programme of computing the inter-ionic potentials for a range of essentially ionic solids is the first step in constructing theoretical models capable of being used to both understand and predict the structures of such encapsulated crystals. Simple

models [35, 36] have yielded insights into the mechanisms through which the ionic crystals fill the tubes when these are immersed in the corresponding ionic liquid melt, the experimental method of preparing the encapsulated solids [27–31].

2. Components of the cohesive energy

2.1. Theoretical overview

The fundamental assumption made in the present calculations is that the crystals are fully ionic. This means [1, 5, 37] that the electronic wavefunction for the entire solid can be written as an anti-symmetrized product of individual ion wavefunctions each of which, although in general different from that of the corresponding free ion, is spherically symmetric and contains the integral number of electrons consistent with its formal charge. The wavefunctions of different ions are not orthogonal; their overlaps generate the short range repulsions which oppose the attractive Madelung terms thereby maintaining crystals at their equilibrium geometries.

For a crystal of stoichiometry CA with closest cation–anion separation R, an expression for the binding energy ($U_{\mathrm{L}}(R)$) measured relative to the sum of those of the free ions is derived [1, 5, 38] by evaluating the energy expectation value predicted from such a crystal electronic wavefunction followed by adding the additional contributions arising from electron correlation. The result, after neglecting the explicitly three-body and higher order multi-body terms expected to be small [37], is

$$U_{\mathrm{L}}(R) = N_f\{-M/R + E_{\mathrm{re}}(R) + n_{\mathrm{CA}}V_{\mathrm{sCA}}(R) + (1/2)[n_{\mathrm{AA}}V_{\mathrm{sAA}}(x_{\mathrm{AA}}R) + n_{\mathrm{CC}}V_{\mathrm{sCC}}(x_{\mathrm{CC}}R)]\} + U_{\mathrm{disp}}(R). \tag{2.1}$$

Here N_f is a constant ensuring that $U_{\mathrm{L}}(R)$ is a binding energy per mol, M is the Madelung constant, $E_{\mathrm{re}}(R)$ is the rearrangement energy needed to convert one free anion into its form optimal for the crystal with cation–anion separation R, n_{XY} is the number of closest neighbouring ions of type Y (Y = cation C or anion A) coordinating one ion of type X and $V_{\mathrm{sXY}}(x_{\mathrm{XY}}R)$ is the short range interaction between one ion X and one closest neighbour of type Y located at a distance $x_{\mathrm{XY}}R$. Each of $E_{\mathrm{re}}(R)$ and the $V_{\mathrm{sXY}}(x_{\mathrm{XY}}R)$ is the sum of an uncorrelated part, designated by the additional superscript ^{0}, plus a contribution originating from electron correlation that is evaluated using simple density functional theory as described elsewhere [12]. Since this method only captures the short range overlap dependent contributions to the correlated part of each $V_{\mathrm{sXY}}(x_{\mathrm{XY}}R)$, the inter-ionic dispersive attractions appear separately in (2.1) with $U_{\mathrm{disp}}(R)$ being the total dispersion energy of the crystal. No cation rearrangement energy appears in (2.1) because there is abundant evidence, reviewed elsewhere [1, 2, 5], that cations having a p^6 outermost electronic configuration are essentially unaffected by their in-crystal environments. However it is well established [1, 2, 5, 7, 10] that anions are contracted by such environments thus introducing non-zero $E_{\mathrm{re}}(R)$ into (2.1). The uncorrelated part ($V^0_{\mathrm{sXY}}(x_{\mathrm{XY}}R)$) of each $V_{\mathrm{sXY}}(x_{\mathrm{XY}}R)$ is computed using the relativistic integrals program (RIP) [39, 40] to yield a result which not only takes full account of relativity but is also exact once given the two individual ion wavefunctions. The methodology used in the present computations differs in only one small detail from that used in the study [12] of CsCl and is fully documented elsewhere [1, 5, 7, 10].

2.2. Short range potentials

The wavefunction for the free cation, needed as input to the RIP program, was computed using the Oxford Dirac–Fock program [41]. For each of the three cubic crystal structures examined, namely the four-coordinated zinc blende (4:4) structure, the 6:6 rock salt structured polymorph and the 8:8 phase having the CsCl structure, the contracted anion wavefunction optimal at each

Table 1. Optimized parameters A and k in the OHSMFS environmental potential (au).

	R	5.5	5.75	6.0	6.125	6.25	6.375	6.5	6.75	7.0	7.5
4:4	A	0.606	0.503	0.435	0.396	0.384	0.363	0.331	0.293	0.258	
	k	2.483	2.309	2.154	2.085	2.068	2.041	2.000	1.900	1.809	
6:6	A	1.92	1.51	1.16	1.04	0.896	0.834	0.780	0.633	0.521	
	k	2.809	2.635	2.431	2.336	2.219	2.185	2.146	2.015	1.876	
8:8	A	8.97	5.94	4.05	3.37	2.85	2.41	2.10	1.59	1.34	0.718
	k	3.869	3.500	3.191	3.082	2.990	2.850	2.776	2.567	2.513	2.011

closest cation–anion separation (R) was computed by introducing an environmental potential into the Dirac–Fock program. This potential describes the interaction of an anion electron (distance r_a from the anion nucleus) with the crystalline environment. In the OHSMFS (optimized hyperbolic secant Madelung Fermi-smoothed [7]) method used here, this potential takes the form [7]

$$F^{(0)}_{\rm env}(r_a;\, R) = A\,{\rm sech}[k(r_a - R)] + F_{\rm MFS}(r_a;\, R). \tag{2.2}$$

Here $F_{\rm MFS}(r_a;\, R)$ is the Fermi-smoothed function representing the Madelung potential [7] and the two constants A and k, which define the short range part, are optimized through an iterative two-step process. In the first step, the anion wavefunction is computed in an OHSMFS environmental potential thus yielding at the Dirac–Fock (uncorrelated level) the rearrangement energy $E^0_{\rm re}(R)$ needed to generate this state of the ion from the free anion. The resulting wavefunction is then input to the RIP program to compute, at the uncorrelated level, the short range two-body energies $V^0_{\rm sXY}(x_{\rm XY}R)$ from which the uncorrelated part ($U^0_{\rm L}(R)$) equation (2.1) of [12])) of $U_{\rm L}(R)$ is calculated. This two-step process is iterated using the variational criterion that the total crystal energy be minimized, which reduces to minimizing the cohesive energy. The resulting values of A and k are reported in table 1. A program RELCRION (Relativistic Crystal Ion Program) incorporating both the RIP and Dirac–Fock programs has been developed to perform these optimizations automatically in a single computation in contrast to the many separate computations required previously. Full details will be reported elsewhere [42]. The OHSMFS method differs from the OEMFS method used to study [12] CsCl only in that the environmental potential is given by (2.2) above rather than by (3.5) of [7]. The OHSMFS and the previously more extensively used OEMFS (optimized on eigenvalues Madelung Fermi-smoothed [6, 7]) and ODMFS (optimized on density Madelung Fermi-smoothed [7]) methods have been shown [7] to yield results of essentially the same quality.

Table 2 presents the uncorrelated parts of the rearrangement energies $E^0_{\rm re}(R)$, short range interactions $V^0_{\rm sCA}(R)$ between each cation and its closest anion neighbour as well as the short range interactions $V^0_{\rm sAA}(x_{\rm AA}R)$ between each anion and its closest anion neighbour at a distance $x_{\rm AA}R$. Both $E^0_{\rm re}(R)$ and $V^0_{\rm sCA}(R)$ increase with both decreasing R in each of the three structures and with increasing coordination number at constant R. This behaviour arises because the anion is becoming increasingly compressed on traversing through either of these sequences as shown by the radial expectation values presented in table 3 for a single outermost electron.

Each total rearrangement energy ($E_{\rm re}(R)$), and short range interaction $V_{\rm sCA}(R)$ and $V_{\rm sAA}(x_{\rm AA}R)$ was derived by adding to the corresponding uncorrelated quantity a short range correlation contribution derived from electron-gas theory. The correlation contribution to each $E_{\rm re}(R)$ was calculated using equation (15) of [10] with the scaling factor $B_{\rm corr}$ having the 0.544 value previously derived [12] for the chloride ion. The short range correlation contributions to the two-body interactions were computed through the method used in all previous studies with the RIP program. Both the uncorrelated and total short range cation–cation interactions

Table 2. Rearrangement energies ($E_{re}(R)$) and anion dependent short range interactions (au). (Note: (1) Each energy without superscript 0 includes the contribution from electron correlation of short range; addition of superscript 0 denotes this contribution is not included. (2) Anion–anion interactions $V^0_{sAA}(x_{AA}R)$ and $V_{sAA}(x_{AA}R)$ are 'optimal'; see text. For the 4:4, 6:6 and 8:8 structures $x_{AA} = \sqrt{(8/3)}$, $\sqrt{2}$ and $[2/\sqrt{3}]$ respectively.)

	$E^0_{re}(R)$			$E_{re}(R)$		
R	4:4	6:6	8:8	4:4	6:6	8:8
5.5	0.013 743	0.031 922	0.051 146	0.010 655	0.027 479	0.045 987
5.75	0.009 270	0.021 224	0.034 696	0.006 735	0.017 676	0.030 462
6.0	0.006 516	0.014 050	0.023 346	0.004 418	0.011 222	0.019 930
6.125	0.005 333	0.011 595	0.018 882	0.003 475	0.009 028	0.015 861
6.25	0.004 530	0.009 404	0.015 275	0.002 858	0.007 103	0.012 609
6.375	0.003 772	0.007 782	0.012 541	0.002 304	0.005 703	0.010 129
6.5	0.003 048	0.006 491	0.010 220	0.001 700	0.004 601	0.008 061
6.75	0.002 159	0.004 352	0.006 894	0.001 073	0.002 869	0.005 161
7.0	0.001 514	0.002 976	0.004 665	0.000 629	0.001 777	0.003 323
7.5			0.002 078			0.001 221
	$V^0_{sCA}(R)$			$V_{sCA}(R)$		
R	4:4	6:6	8:8	4:4	6:6	8:8
5.5	0.022 772	0.019 318	0.016 801	0.020 690	0.017 453	0.015 057
5.75	0.015 735	0.013 438	0.011 657	0.014 053	0.011 914	0.010 238
6.0	0.010 863	0.009 399	0.008 155	0.009 510	0.008 156	0.006 996
6.125	0.009 078	0.007 857	0.006 874	0.007 860	0.006 739	0.005 823
6.25	0.007 549	0.006 595	0.005 794	0.006 458	0.005 587	0.004 841
6.375	0.006 307	0.005 521	0.004 868	0.005 325	0.004 615	0.004 011
6.5	0.005 298	0.004 619	0.004 106	0.004 419	0.003 806	0.003 332
6.75	0.003 708	0.003 272	0.002 915	0.003 001	0.002 613	0.002 288
7.0	0.002 610	0.002 318	0.002 080	0.002 043	0.001 786	0.001 569
7.5			0.001 076			0.000 744
	$V^0_{sAA}(x_{AA}R)$			$V_{sAA}(x_{AA}R)$		
R	4:4	6:6	8:8	4:4	6:6	8:8
5.5	0.000 104	0.000 441	0.003 789	0.000 027	0.000 260	0.002 856
5.75	0.000 061	0.000 296	0.002 547	−0.000 001	0.000 137	0.001 735
6.0	0.000 036	0.000 196	0.001 704	−0.000 011	0.000 058	0.000 990
6.125	0.000 027	0.000 158	0.001 389	−0.000 014	0.000 032	0.000 716
6.25	0.000 021	0.000 127	0.001 125	−0.000 014	0.000 010	0.000 492
6.375	0.000 016	0.000 101	0.000 912	−0.000 015	−0.000 005	0.000 326
6.5	0.000 012	0.000 080	0.000 732	−0.000 014	−0.000 015	0.000 185
6.75	0.000 007	0.000 050	0.000 468	−0.000 013	−0.000 028	−0.000 001
7.0	0.000 004	0.000 031	0.000 287	−0.000 011	−0.000 033	−0.000 118
7.5			0.000 103			−0.000 188

reported in table 4, being computed from the free cation wavefunction, are independent of structure.

2.3. The anion–anion interaction

The anion–anion potentials reported in table 2 are called 'optimal [43, 44] because, for all three structures, each interaction at each R was computed using the wavefunction optimal for

Table 3. Chloride ion properties (au). (Note: Mean radius and mean square radius in au are averages with weights of 1/3 and 2/3 over those for the relativistic orbitals $3p_{1/2}$ and $3p_{3/2}$ having $j = 1/2$ and 3/2 respectively.)

	$\langle r \rangle$			$\langle r^2 \rangle$			$\langle r^4 \rangle$		
R	4:4	6:6	8:8	4:4	6:6	8:8	4:4	6:6	8:8
6.0	1.971	1.953	1.939	4.688	4.560	4.469	42.095	37.930	35.361
6.25	1.982	1.966	1.957	4.757	4.644	4.579	44.083	40.287	38.122
6.375	1.987	1.971	1.963	4.792	4.680	4.619	45.117	41.337	39.224

Table 4. The short range Rb^+–Rb^+ interaction (au).

$x_{CC}R$	$V^0_{sCC}(x_{CC}R)$	$V_{sCC}(x_{CC}R)$	$x_{CC}R$	$V^0_{sCC}(x_{CC}R)$	$V_{sCC}(x_{CC}R)$
$[2/\sqrt{3}]$ 5.5	0.002 054	0.001 642	7.0$[2/\sqrt{3}]$	0.000 041	0.000 004
$[2/\sqrt{3}]$ 5.75	0.001 092	0.000 807	5.75$\sqrt{2}$	0.000 036	0.000 003
$[2/\sqrt{3}]$ 6.0	0.000 574	0.000 380	6.0$\sqrt{2}$	0.000 016	−0.000 003
$[2/\sqrt{3}]$ 6.125	0.000 416	0.000 256	6.125$\sqrt{2}$	0.000 010	−0.000 005
$[2/\sqrt{3}]$ 6.25	0.000 299	0.000 168	6.25$\sqrt{2}$	0.000 007	−0.000 004
$[2/\sqrt{3}]$ 6.375	0.000 217	0.000 110	6.375$\sqrt{2}$	0.000 004	−0.000 004
$[2/\sqrt{3}]$ 6.5	0.000 155	0.000 067	6.5$\sqrt{2}$	0.000 003	−0.000 003
5.5$\sqrt{2}$	0.000 083	0.000 024	5.75$\sqrt{(8/3)}$	0.000 001	−0.000 003
$[2/\sqrt{3}]$ 6.75	0.000 080	0.000 022	7.0$\sqrt{2}$	0.000 000	−0.000 002

that crystal geometry. Potentials $V^0_{sAA}(r_{AA})$ and $V_{sAA}(r_{AA})$ computed using at all inter-ionic separations the same anion wavefunction, namely that optimal for an R value, denoted R'_e, close to the equilibrium value R_e are called 'frozen' [43–45]. Here r_{AA} is the anion–anion separation.

Frozen potentials are required for current implementations of the compressible ion model which have been reviewed elsewhere [2, 43]. For RbCl, the uncorrelated and total frozen anion–anion potentials computed from the Cl^- wavefunction for the 6:6 structure with $R'_e = 6.25$ au are presented and discussed in the appendix.

2.4. The dispersion energy

The total two-body dispersion energy, $U_{disp}(R)$, appearing in (2.1), including its damping at inter-ionic separations for which the overlap of the ion wavefunctions ceases to be negligible, was calculated using the methods already described [5, 7, 9, 10]. The values of the dipole–quadrupole dispersion coefficients, $C_8(CC)$, $C_8(AA)$, $C_8^{DQ}(CA)$ and $C_8^{QD}(CA)$ derived from the Starkschall–Gordon formula, were scaled as before for CsCl using the same factors [12] of 1.403, 1.285, 1.352 and 1.394. The total Axilrod–Teller triple dipole dispersion energy, $U_{AT}(R)$, of the crystal was evaluated, as previously [12], in its undamped form. The significance of this interaction is assessed here by adding it, at each R value, to the expression (2.1) for $U_L(R)$.

All the data needed to evaluate both the two-body dispersion energy and the Axilrod–Teller energy for interactions involving only the cations are presented in table 5. The value of the Rb^+ polarizability, α_C, was derived [46] from experimental data and subsequently confirmed by an independent *ab initio* quantum chemistry electronic structure computation [47]. The electron number, P_C, needed to calculate the $C_6(CC)$ coefficient from the Slater–Kirkwood formula was derived [5] from data on the iso-electronic inert gas.

Table 5. Cation properties and purely cationic dispersion coefficients (au).

α_C	P_C	d_C	$\langle r^2\rangle_C$	$\langle r^4\rangle_C$	C_6(CC)	C_8(CC)	ν(CCC)
9.05	7.305	2.282	20.454	115.899	55.188	1316.209	374.857

Table 6. Anion dependent polarizabilities and parameters determining the two-body dispersive attractions (au).

	α_A	P_A	d_A	C_6(CA)	C_6(AA)	C_8(AA)	C_8^{DQ}(CA)	C_8^{QD}(CA)
4:4	25.476	6.106	1.605	109.592	238.307	8249.705	1995.832	1298.477
6:6	23.409	6.106	2.073	103.476	209.907	7019.565	1820.399	1226.013
8:8	23.697	6.106	2.220	104.340	213.786	6998.067	1796.773	1236.250

Table 7. Anion dependent three-body triple dipole dispersion coefficients (au).

	ν(CCA)	ν(CAA)	ν(AAA)
6:6	766.761	1650.128	3635.363
8:8	773.826	1682.594	3799.565

The two-body dispersion interactions involving anions are structure dependent and the data needed for their evaluation are assembled in table 6. The anion polarizability, α_A, for the 6:6 structure at its experimental equilibrium R value, denoted R_e, was derived by subtracting α_C from the experimental molar polarizability [48] of 32.459 au. There is no experimental value for the polarizability of the Cl^- ion in either the 4:4 or 8:8 phase at their respective equilibrium geometries. These polarizabilities were therefore derived from the semi-empirical yet trustworthy relation [46]

$$\log_{10}\alpha_A = A + BR_e^{-2} + CR_e^{-4} \tag{2.3}$$

which describes the dependence on R_e of the polarizabilities of anions in crystals at their equilibrium geometries. The coefficients A, B and C are the same for the 6:6 and 8:8 phases, those labelled P for parabolic fit in table 3 of [46] being used to derive α_A for the latter phase. For RbCl, the reliability of (2.3) is confirmed by its prediction of an α_A value of 23.451 au for the 6:6 phase taking R_e to have the room temperature value of 6.219 au used to derive the A, B and C coefficients. The value of R_e input to (2.3) in the derivation of α_A for the 8:8 phase was that predicted by the RIP computation, described in the next section, using the dispersion parameters of the 6:6 structure. The values of the coefficients in (2.3) do not transfer from the 6:6 and 8:8 phases to the 4:4 structure [49]. The anion polarizability in this structure was therefore predicted from the linear ($C = 0$) form of (2.3) using the coefficients A and B derived for this structure which are presented under the heading 'linear B3' in table 5 of [49]. The R_e value used was that predicted by the RIP computation with the dispersion parameters of the 6:6 structure.

For each of the 4:4, 6:6 and 8:8 phases, the two anion expectation values $\langle r^2\rangle$ and $\langle r^4\rangle$ (table 3) for the R value closest to R_e were used to derive the dipole–quadrupole dispersion coefficients from the Starkschall–Gordon formula. These R values were 6.0, 6.25 and 6.5 au respectively. The ν(XXY) triple–dipole dispersion coefficients involving anions and assembled in table 7 were derived from the Midzuno–Kihara formula using the polarizabilities and dipole–dipole dispersion coefficients presented in tables 5 and 6.

Table 8. Crystal cohesion predicted for three cubic structures. (Note: (1) Lattice energy D_e in kJ mol^{-1}, equilibrium closest cation–anion separation R_e in au. (2) Compressibility B in 10^{10} N m^{-2}. (3) Experimental D_e at 0 K from [67–69]; R_e at 0 K from [50] and B at 4.2 K from [70]. (4) See text for comparison with experiment of the R_e computed for the 8:8 phase.)

	4:4	6:6			8:8	
	$U_L(R)$	$U_L(R)$	$+U_{AT}(R)$	Expt	$U_L(R)$	$+U_{AT}(R)$
D_e	648.5	687.6	684.3	689, 692, 695	694.0	687.7
R_e	6.099	6.214	6.239	6.172	6.324	6.371
B	1.055	1.881	1.874	1.865	2.498	2.304

Table 9. Influence of chloride ion description on the predicted crystal binding. (Note: See notes (1) and (2) to table 8.)

	4:4			6:6		8:8			
	6:6 $U_{disp}(R)$	Frozen $V_{sAA}(r_{AA})$	$U_L(R)$	Frozen $V_{sAA}(r_{AA})$	$U_L(R)$	All 6:6 pots	6:6 $U_{disp}(R)$	Frozen $V_{sAA}(r_{AA})$	$U_L(R)$
D_e	651.8	648.3	648.5	687.6	687.6	690.8	691.9	693.7	694.0
R_e	6.054	6.098	6.099	6.206	6.214	6.394	6.342	6.308	6.324
B	1.024	1.025	1.055	1.854	1.881	2.330	2.443	2.594	2.498

Table 10. Predicted differences (ΔU_8) between the 6:6 and 8:8 structure energies (kJ mol^{-1}). (Note: For full definition of methods, see the text; the first four results do not include $U_{AT}(R)$ or U_{ZP}.)

Method	All 6:6 pots	6:6 $U_{disp}(R)$	Frozen $V_{sAA}(r_{AA})$	$U_L(R)$	$U_L(R)$ + $U_{AT}(R)$	$U_L(R)$+ $U_{AT}(R)$ + U_{ZP}
ΔU_8	3.2	4.3	6.1	6.4	3.4	3.2

3. Cohesion of the three cubic phases

3.1. The relative energies of the polymorphs

The lattice energy D_e, positive for a bound crystal, R value R_e at which the crystal binding is maximized and the bulk compressibility B were predicted for each of the three phases by considering the R dependence of the crystal binding energy $U_L(R)$ (2.1). This is the energy expression derived by including not only all explicitly two-body terms but also the implicitly multi-body effects that arise from the modification of the anion wavefunction through its interaction with all the other ions in the crystal. These effects not only generate a finite rearrangement energy but also produce short range interactions optimal for the in-crystal environment. It is only the explicitly three-body and higher order multi-body terms, the mathematical expressions for all of which involve the wavefunctions of three or more ions, that are not included in $U_L(R)$ [1, 5]. Since the Axilrod–Teller three-body interaction makes a small but significant contribution [12] to the difference between energies of the 6:6 and 8:8 phases of CsCl, this interaction was also considered here. The results of those RbCl computations which included these interactions are reported in the columns labelled '$+U_{AT}(R)$' in tables 8–10.

The reliability of the present computations is shown by the good agreement (table 8) between experiment and the theoretical predictions, both without and with the small contribution from $U_{AT}(R)$, for the cohesive properties D_e, R_e and B for the 6:6 structure

of RbCl. This is the only phase of RbCl for which there is unambiguous experimental data. The prediction that D_e for the 4:4 structure is 39 kJ mol^{-1} smaller than that of the 6:6 phase, coupled with the greater molar volume of the former, explains the lack of experimental evidence for this polymorph.

The theoretical result (both with and without the inclusion of $U_{AT}(R)$) that D_e for the 8:8 structure is larger than that for the 6:6 phase predicts quite unambiguously that the 8:8 phase lies at a lower energy than the 6:6 structure. Although these calculations did not include the short range interactions between second nearest neighbour anion pairs, namely those separated at respective distances of $2R$ and $2R\sqrt{(2/3)}$ in the 6:6 and 8:8 phases, the result that $V^0_{sAA}[2R\sqrt{(2/3)}]$ was found to be only 0.000 005 au and 0.000 004 au for $R = 6.25$ and 6.375 au in the 8:8 structure shows that the larger D_e predicted for this phase is not an artefact caused by omitting these more distant interactions. Furthermore, both of the corresponding total short range interactions $V_{sAA}[2R\sqrt{(2/3)}]$ were found to be only $-0.000\,001$ au. The prediction that the 8:8 phase has the larger D_e inevitably carries the further implication that this phase is the most stable at 0 K even though only the 6:6 structure is observed at ambient temperatures. This provides very strong support to the experimental evidence [23, 24] that the 8:8 phase is indeed the most stable at low temperatures. Thus it has been reported [23] that, although condensing RbCl in a glass capillary at $-190\,^{\circ}$C produces the 6:6 structure, condensation onto a previously deposited layer of TlCl produces the 8:8 phase at $-190\,^{\circ}$C but the 6:6 structure at room temperature. All further layers deposited at $-190\,^{\circ}$C exhibited the 8:8 structure. It was therefore argued [23] that the 8:8 phase really is the most stable at $-190\,^{\circ}$C and it was not generated merely because it was initially condensed onto a template having the same structure. The conversion of the 8:8 phase of RbCl into the 6:6 phase by heating provided further evidence for the temperature dependence of the relative stability of these two phases. The step rule [25, 26] can explain why the 6:6 structure, rather than the thermodynamically stable 8:8 phase, was produced in the direct condensation onto glass at $-190\,^{\circ}$C. The production [24] of the 8:8 polymorph by condensation of RbCl onto amorphous bases at low temperatures is further evidence that this phase has the lowest energy. However, it should be noted that the experimental measurements [23, 24] also provide evidence for disorder within the thin films studied, and moreover that the diffraction images are diffuse, consistent with the presence of small nuclei of both structural types. The value of 6.124 au reported [23] as measured by x-ray diffraction for the R_e value of the 8:8 phase is not only inconsistent with the later electron diffraction result [24] of 6.497 ± 0.20 au but also the smaller result does not appear to be a credible reflection of the true bulk value since it is less than the well established [50] 6.172 au R_e of the 6:6 phase. However, as already noted, the electron diffraction data for RbCl consists of diffuse rings with large associated measurement errors. Furthermore, the low temperature data presented in [23] may be polluted by the presence of ice on the sample. The further experimental result [50] that R_e for the 8:8 phase under a pressure of 5 kbar is 6.399 au is more evidence that the 6.172 au result cannot be representative of the bulk material. The agreement of the predictions (table 8), both with and without including $U_{AT}(R)$, for the R_e of the 8:8 phase with the 6.497 ± 0.20 au experimental value [24] provides further evidence that the results of the present calculations are trustworthy.

The results assembled in table 8 show that the difference ΔU_8 between the lattice energies of the 8:8 and 6:6 structures, defined to be positive if D_e is larger for the former phase, is predicted to be 3.4 kJ mol^{-1} after introduction of the Axilrod–Teller energy. The results from the similar study [12] for CsCl indicate that this 3.4 kJ mol^{-1} prediction is more reliable than the larger value of 6.4 kJ mol^{-1} derived without considering $U_{AT}(R)$, that is from just $U_L(R)$ (2.1). The zero point energy U_{ZP} of each of the 6:6 and 8:8 RbCl phases was calculated using the GULP program and the shell model as described in section 4 below. Since U_{ZP} for

the 8:8 phase was only predicted to be 0.2 kJ mol^{-1} greater than that of the 6:6 structure, the resulting 3.2 kJ mol^{-1} for ΔU_8 remains essentially unaltered from that derived by considering just the sum $U_L(R) + U_{AT}(R)$.

3.2. Analysis of the cohesive energies

3.2.1. Dependence on differences between the anion wavefunctions. The small size of the energy difference ΔU_8 shows the need to investigate whether the predicted crystal cohesion is sensitive to the way in which the in-crystal anion is described. The significance of using the potential fully optimal for the phase considered is shown by the comparison (table 9) between the results thereby predicted with those derived using slightly different potentials. For each of the three phases, the predictions in the columns headed '$U_L(R)$' derived using the optimal potentials differ only very slightly from those in the columns headed 'frozen $V_{sAA}(r_{AA})$' derived using the frozen anion–anion interaction reported in seventh column of potentials in table A.1. However, the cohesion predicted for the 4:4 and 8:8 phases shows slightly greater discrepancies with the fully optimal results if the dispersion energy $U_{disp}(R)$ is calculated using the dispersion parameters of the 6:6 structure rather than those appropriate for the phase considered. These D_e values, presented in the columns headed '6:6 $U_{disp}(R)$' in table 9, differ from their fully optimal counterparts by about 3 kJ mol^{-1}. The results for the 8:8 phase reported in the columns headed 'all 6:6 pots' were derived with all the potentials taken from the 6:6 structure except for using the frozen potential for $V_{sAA}(r_{AA})$. This approximation loses a further 1 kJ mol^{-1} of lattice energy.

The results presented in table 10 show how the prediction for ΔU_8 is influenced by the chosen potential model. The results in the first four columns show how the calculated ΔU_8 increases on passing from using the 6:6 phase potentials for 8:8 phase to that predicted using for each phase the potentials optimal for that phase. Although introducing $U_{AT}(R)$ significantly reduces the predicted ΔU_8, this is still unambiguously predicted to be positive.

3.2.2. Significance of the dispersion energy. Both previous theoretical investigations [6, 12, 14, 15] of the lattice energies of the 6:6 and 8:8 phases of CsCl as well as the values of $U_{disp}(R)$ computed here for RbCl show that one cannot hope to predict correctly even the sign of ΔU_8 unless the dispersion energy is considered. Thus ΔU_8 is predicted to be -7.6 kJ mol^{-1} for CsCl [12] if the dispersion energy is neglected, with furthermore the cohesion of both of the individual phases being significantly underestimated as manifested by predictions for D_e that are too small coupled with overestimated R_e values. The dispersive attractions were found not only to be responsible for the underestimation of the individual cohesions of the two phases but also, more importantly, to contribute +15.5 kJ mol^{-1} to ΔU_8 to produce a final prediction for ΔU_8 of +7.9 kJ mol^{-1} [12]. The agreement with the experimental value of 5.6 kJ mol^{-1} is most acceptable in view of the small size of this energy difference.

The importance of the dispersion contribution to ΔU_8 is further shown by the -12.6 kJ mol^{-1} prediction [51] for CsCl yielded by a density functional (DFT) computation of the type which, using purely local energy functionals (local density approximation LDA), does not capture the dispersive attractions. In the comparison with experiment of the predicted cohesion of the one (8:8) phase stable at room temperature, the absence of dispersion was partially masked because the LDA description yields inter-ionic exchange attractions that are too great in magnitude. This was first emphasized by Rae [52, 53], subsequently discussed from a slightly different perspective [1, 54] and more recently reiterated from a third viewpoint [55]. Thus, although the R_e of 6.710 au calculated [51] for the 8:8 phase of CsCl is not unreasonable

when compared with the experimental result of 6.748 au [16], the partial cancellation of the error of lack of dispersion with that of too attractive exchange cannot be expected to occur to the same degree in two different phases. This, therefore, renders untrustworthy the ΔU_8 predictions of such computations. This shows that a calculation for RbCl which does not include dispersion, and which only obtains reasonable results for its 6:6 phase because the lack of dispersion is partially compensated by too attractive an exchange, will not predict ΔU_8 reliably. Thus for RbCl, the computations [51] predicted ΔU_8 to be -13.1 kJ mol^{-1} even though the R_e and B values of 6.208 au and 1.66×10^{10} N m^{-2} calculated for the 6:6 phase are reasonable when compared with their experimental counterparts presented in table 8.

The earlier density functional calculations [56] of the Gordon–Kim type [57], in which both an additive density assumption and a Thomas–Fermi–Dirac treatment of the kinetic energy were introduced in addition to the LDA exchange, predicted ΔU_8 for RbCl to be -9.6 kJ mol^{-1}. This result is qualitatively similar to the later DFT result of -13.1 kJ mol^{-1} [51]. Furthermore, the overattractive exchange in the calculation [56] partially compensated not only for the absence of dispersion but also for the use of the wavefunction of the free chloride ion which has been shown subsequently [5, 12, 58] to overestimate the short range cation–anion repulsion. These errors very largely cancelled to predict $D_e = 690$ kJ mol^{-1}, $R_e = 6.16$ au and $B = 1.85 \times 10^{10}$ N m^{-2} in very reasonable agreement compared with experiment (table 8). The Waldman–Gordon factors [59, 60] used [56] to correct errors in the kinetic and exchange functionals, although largely successful for light ions, fail to improve more than very marginally the results for heavier systems for which these factors remain close to unity for the reasons described elsewhere [1]. The error cancellations in the calculations [56] explain why a later computation [61] using an improved description of the in-crystal anion, thus reducing the short range cation–anion repulsion whilst still retaining the overattractive exchange and no dispersion, predicted too small an R_e value of 6.038 au. The prediction of 6.530 au [61] for R_e in the 8:8 phase of CsCl similarly underestimates the experimental result of 6.748 au [16]. Clearly the -11.4 kJ mol^{-1} prediction [61] for ΔU_8 of RbCl cannot be trusted.

The present calculations predict the total crystal dispersion energy ($U_{\text{disp}}(R)$) of RbCl in the 6:6 and 8:8 phases to be -90.5 and -92.9 kJ mol^{-1} respectively at $R = 6.25$ au. These results, typical of those for RbCl close to the equilibrium geometries, provide conclusive evidence that the dispersive attractions play a significant role in its cohesion and hence they must be considered in any trustworthy calculations of its properties.

4. Shell model description

It is well established [2] that ion-induced dipole interactions can be important in the energetics of ionic materials when ions do not reside on centres of symmetry. Since a significant fraction of the ions in an encapsulated nanocrystal are located in such sites, the potentials computed for cubic materials must be augmented with a description of such a polarization response. This is conveniently described by using the shell model which has not only been thoroughly documented in the literature but can also be readily implemented because it is incorporated into the GULP program [62].

The GULP program can handle two-body interactions in both numerical and a range of analytic forms as well as the undamped Axilrod–Teller interaction. Since, however, it does not handle compressible ion models and rearrangement energies, it was necessary to introduce, for each of the cubic phases, the short range cation–anion effective pair potential ($V_{\text{sCA}}^{\text{eff}}(R)$) defined by

$$V_{\text{sCA}}^{\text{eff}}(R) = V_{\text{sCA}}(R) + (1/n_{\text{CA}})E_{\text{re}}(R). \tag{4.1}$$

Table 11. Fitted short range interactions and predicted 6:6 phase crystal cohesion (au). (Note: Constants A_1, b_1, A_2 and b_2 defined by equation (4.1).)

	Analytic potentials					Predicted cohesion[a]		
	A_1	b_1	A_2	b_2	χ^2		Fitted	RIP
$V^{\text{eff}}_{\text{CA}}(R)$	13.7581	0.578 212	115.031	0.639 93	1.8361×10^{-10}	D_e	684.3	684.3
$V_{\text{sAA}}(r_{\text{AA}})$	3.893 57	1.080 63	−1.873 84	1.185 25	4.781×10^{-11}	R_e	6.238	6.239
$V_{\text{sCC}}(r_{\text{CC}})$	170 958.0	0.351 755	−0.061 54	0.961 563	3.942×10^{-11}	B	1.793	1.874

[a] Includes $U_{\text{AT}}(R)$ but excludes U_{ZP}. See notes (1) and (2) to table 8.

This definition ensures [6, 12] that the expression (2.3) of [12] for $U_{\text{L}}(R)$ is reproduced if (4.1) is taken to be the short range cation–anion interaction in standard expressions for the crystal energy which do not contain a rearrangement term. Both $V_{\text{sCC}}(r_{\text{CC}})$ and, for the 6:6 phase, $V^{\text{eff}}_{\text{sCA}}(R)$ and $V_{\text{sAA}}(r_{\text{AA}})$ were fitted to the analytic form

$$V'_{\text{sXY}}(r_{\text{XY}}) = A_1 \exp(-b_1/r_{\text{XY}}) + A_2 \exp(-b_2/r_{\text{XY}}) \tag{4.2}$$

where $V'_{\text{sXY}}(r_{\text{XY}})$ is $V^{\text{eff}}_{\text{sCA}}(R)$ for the X = C, Y = A case but is just the short range two-body interaction when either X = Y = C or X = Y = A. Table 11 presents, for each of the three potentials, the four defining parameters in (4.2) along with the χ^2 value describing the quality of the fit. The presence of the weak attractive tails, arising from the short range correlation contributions, in both $V_{\text{sCC}}(r_{\text{CC}})$ and $V_{\text{sAA}}(r_{\text{AA}})$ clearly means that these potentials could not be fitted with just a single exponential. It was also found that $V^{\text{eff}}_{\text{sCA}}(R)$ could not be described sufficiently accurately by a single exponential. It is beyond the scope of this paper to elucidate the reasons for the failure of a single exponential description. However, two possibilities are first, that the two components $V_{\text{sCA}}(R)$ and $E_{\text{re}}(R)$ of $V^{\text{eff}}_{\text{sCA}}(R)$ might have different distance dependencies, and second that $V_{\text{sCA}}(R)$ itself is the sum of penetration and permutation components as discussed for the anion–anion interaction in the appendix.

The dispersive attractions between each type of ion pair were input in numerical form to the GULP program because this does not currently incorporate the dispersion damping functions used in the present work. Since, however, these damping functions are analytic, the dispersive attractions could be computed at as many inter-ionic separations as were needed to ensure that only negligible errors arose from their description in the GULP program by spline functions. The results presented in the right-hand side of table 11 show that the values of D_e, R_e and B computed using the fitted potentials (4.2) and the GULP program agree well with their counterparts (table 8) calculated directly by using the Simons, Parr, and Finlan analysis [63] of the R dependence of the predicted crystal cohesion. However, the results derived using a $V^{\text{eff}}_{\text{sCA}}(R)$ fitted to just a single exponential failed to reproduce to an acceptable level of accuracy the *ab initio* results in table 8.

The shell model requires defining, for each ion X, the shell charge Y_{X} and spring constant k_{X}. These yield the polarizability of the isolated ion as $(Y_{\text{X}})^2/k_{\text{X}}$. A first plausible approach to defining these parameters in a non-empirical way is, for each ion, to take $|Y_{\text{X}}|$ to equal the electron number (tables 5 and 6) used to derive the dipole–dipole dispersion coefficients and then to calculate k_{X} by demanding that the polarizability of that ion is reproduced. This approach was adopted for the cation, taking the polarizability to be that of the free ion. Since anions, unlike alkali cations, are significantly affected by their environment in-crystal, the value of the anion polarizability to be used is not obvious *a priori*. This uncertainty is compounded because the shell model does include a description of some of the in-crystal modifications generated by the short range forces. However, it was found that, if the anion spring constant

Table 12. The elastic constants, zero point energy and entropy of the 6:6 phase. (Note: Elastic constants in 10^{10} N m^{-2} and entropy (S) at 298 K in J K^{-1} mol^{-1}.)

Method	$U_L(R)$	$U_L(R)+U_{AT}(R)$		$U_L(R)$	$U_L(R)+U_{AT}(R)$	Expt[a]
Y_A (au)	−3.4	−3.1	C_{11}	4.340	4.145	4.297
k_A (au)	0.477	0.394	C_{12}	0.557	0.617	0.649
U_{ZP} (kJ mol^{-1})	3.45	3.39	C_{44}	0.557	0.617	0.493
			S	92.9	93.7	95.9

[a] Experimental elastic constants at 4.2 K from [70] and experimental entropy from [64].

k_A was derived from either the polarizability of the free ion or that of the ion in a point charge lattice, then the experimental molar total crystal polarizability α_{cr} (=32.459 au [48]) was not reproduced. The resulting values of α_{cr} were too large, so that the high frequency dielectric constant ε_∞, determined by α_{cr} through the Clausius–Mossotti relation, was also overestimated. It was therefore decided to determine k_A by demanding that the experimental α_{cr} be reproduced. Since the Clausius–Mossotti equation relating α_{cr} and ε_∞ also contains the molar volume, adjusting k_A to reproduce α_{cr} will only also reproduce ε_∞ if the computation perfectly predicts the experimental R_e. Since the GULP program directly yields ε_∞ rather than α_{cr}, it was required that the program predicted the ε_∞ which yields the correct α_{cr} using the predicted rather than the slightly different experimental R_e in the Clausius–Mossotti equation. However, it was found that, whether k_A was determined by fitting to either α_{cr} or ε_∞, the static dielectric constant ε_0 was predicted to be 5.597 compared with the experimental value [64] of 4.91. Since it is ε_0 which determines the response of the crystal to an externally applied static electric field and, furthermore, ions in encapsulated crystals will experience such fields, we believe that it is essential that a shell model description of such ions is only suitable for studying encapsulated crystals if it reproduces ε_0. However, it was found that changing Y_A from $-P_A$ whilst still determining k_A by requiring that ε_∞ was reproduced, predicted a different value for ε_0. The parameters Y_A and k_A, presented in table 12, were therefore determined by requiring that the experimental values of both α_{cr} and ε_0 were simultaneously reproduced. Slightly changed Y_A and k_A values result when these are similarly determined with the Axilrod–Teller interactions introduced in the calculation of the crystal energy. Although Y_A is considerably smaller in magnitude than either P_A or the common $|Y_C|$ and P_C of the cation, such Y_C and Y_A values are qualitatively similar to those determined by empirical fitting for both alkali halides [65] and CaF_2 [66].

The entropy at 300 K, the zero point energy and elastic constants at 0 K computed for the 6:6 phase are compared in table 12 with the available experimental data. These predictions agree well with experiment. The two elastic constants C_{12} and C_{44} are predicted to be equal because the use in the GULP program of effective potentials of the type (4.1) reduces the expression for the total energy of the crystal to a sum of pair potentials. The cancellation of errors in the early electron gas computations [56] are retained in their predictions for C_{11} and C_{12} (=C_{44}) of 4.18×10^{10} and 0.69×10^{10} N m^{-2}. The treatment of the lattice dynamics [61] is, in principle, more sophisticated because this includes one of the mechanics that can destroy the equality between C_{12} and C_{44}. However, the resulting predictions of 3.923×10^{10} N m^{-2}, 0.633×10^{10} N m^{-2} and 0.650×10^{10} N m^{-2} for C_{11}, C_{12} and C_{44} respectively, readily deduced from the combinations presented in [61], are less satisfactory than those presented in table 12. Even the sign of the difference $C_{11}-C_{44}$ is predicted incorrectly.

For the 8:8 phase, the short range interactions involving the anions were also described by using the spline functions incorporated in the GULP program. Since there is no experimental value of ε_0 for this phase, Y_A was taken to be the same as that for the 6:6 polymorph. However,

Table 13. The elastic constants, zero point energy and entropy of the 8:8 phase. (Note: See note to table 12.)

Method	$U_L(R)$	$U_L(R)+U_{AT}(R)$		$U_L(R)$	$U_L(R)+U_{AT}(R)$
Y_A (au)	−3.4	−3.1	C_{11}	6.206	5.836
k_A (au)	0.470	0.389	C_{12}	1.451	1.335
U_{ZP} (kJ mol^{-1})	3.75	3.58	S	87.9	90.2

addition of α_C to the α_A result (table 7) derived in section 2.3 for the 8:8 phase yields the reliable value of 32.747 au for α_{cr}. The k_A value, presented in table 13, was therefore derived by requiring that this α_{cr} value was reproduced. This approach predicted ε_0 to be 7.487 without $U_{AT}(R)$ and 7.668 including $U_{AT}(R)$. Very similar values of 7.431 and 7.618 result if both Y_A and k_A are taken to remain unchanged from the 6:6 phase. The entropy at 300 K, zero point energy and elastic constants (table 13) predicted using the optimal Y_A and k_A values are essentially identical to those derived using the shell parameters of the 6:6 phase. The prediction that the entropy of the 8:8 phase is smaller than that (table 12) of the 6:6 polymorph explains why the latter is the more stable at higher temperatures even though the former has a lower energy.

5. Conclusion

This paper has presented a non-empirical fully ionic description of three cubic polymorphs of solid rubidium chloride, these being a four-coordinated phase having the zinc blende structure, the six-coordinated material having the rock salt structure and the eight-fold coordinated phase having the cesium chloride structure. Compressed yet still spherically symmetric wavefunctions optimal for the anion in each in-crystal environment were computed by using a version of the Oxford Dirac–Fock program slightly modified by including the OHSMFS description for the part of the potential that originates from all the other ions and which acts on each anion electron. These in-crystal anion wavefunctions and the free cation Dirac–Fock wavefunction were used to compute, with the Relativistic Integrals Program in its automated RELCRION form, uncorrelated two-body inter-ionic interaction potentials which are exact once the input wavefunctions have been specified.

The inter-ionic potentials and rearrangement energies needed to convert a free anion into their optimal in-crystal forms computed at both the uncorrelated level and with the inclusion of the short range correlation corrections have been reported in detail. These are needed both for parameterizing compressible ion models and for constructing effective cation–anion interactions. At least one of these two sets of potentials could then be used to describe the structures of small RbCl clusters either in isolation or as a small nanocrystal encapsulated in a nanotube. The 'optimal' anion–anion short range potentials, computed by using at each inter-nuclear separation the Cl^- wavefunction optimal for that geometry, have been compared with the corresponding 'frozen' potential in which the same anion wavefunction, one optimal for a near equilibrium cation–anion separation (R'_e), is used to compute the potential over the entire range of inter-anionic distances. This comparison shows at all distances, except at the largest R for the optimal 8:8 potential, the behaviour designated 'normal' [43, 44] in which the optimal potential is less repulsive that its frozen counterpart for R less than R'_e, becoming more repulsive at larger R. The opposite behaviour, designated mixed, arises in the comparison involving the optimal 8:8 potential at the largest R values.

The lattice energy predicted for the 4:4 structure is almost 40 kJ mol^{-1} smaller than that calculated for either the 6:6 or the 8:8 polymorph. This provides an explanation, in

addition to traditional radius ratio arguments, for the lack of experimental evidence for the four-coordinated phase. The present computations clearly predict that the 8:8 phase lies lower in energy by some 3 kJ mol^{-1} than the 6:6 structure not withstanding that it is the latter phase which is the most stable at room temperature. The prediction that the 8:8 phase is energetically favoured is not only consistent with radius ratio arguments but, more significantly, is supported by two separate experiments [23, 24] that strongly suggest that this phase is indeed favoured over the 6:6 structure at low temperatures. Good evidence that the present calculations are trustworthy is provided both by the good agreement between the predicted and well established experimental results for the cohesive properties of the 6:6 polymorph and by the success of computations [6, 12] of the present type in explaining and predicting the greater stability of the 8:8 phase of CsCl compared with the 6:6 polymorph. The importance of the contributions of the inter-ionic dispersive attractions to differences between the energies of the different phases has been re-emphasised.

A shell model, suitable through its incorporation of ion-induced dipole interactions, for describing both small clusters and crystals encapsulated in nanotubes has also been presented. The cation shell parameters were defined by combining a simple theoretical argument with the known value of the electronic polarizability of the free cation. The anion parameters were derived by using the requirement that both the total electronic polarizability and the static dielectric constant of the bulk crystal are reproduced. Both the elastic constants and the entropy predicted for the 6:6 phase at 300 K agree well with experiment. The smaller entropy predicted for the 8:8 structure explains the greater stability and experimental observation of the 6:6 phase at ambient temperatures even though its energy is not quite as low as that of the 8:8 polymorph.

Acknowledgments

We would like to thank the Leverhulme foundation for providing financial support which included that of Dr Shreyas Y Bhide, whom we thank for assistance with performing the computations.

Appendix. Comparative analysis of the optimal and frozen anion–anion potentials

In table A.1, the fifth potential is the uncorrelated 'frozen' short range anion–anion interaction computed by using at all r_{AA} the same anion wavefunction, that optimal for the 6:6 structure having an R (denoted R'_e) of 6.25 au, close to the experimental R_e of 6.172 au. The rightmost column contains the corresponding total short range interaction. Each frozen $V^0_{sAA}(r_{AA})$ and $V_{sAA}(r_{AA})$, whether reported as 4:4, 6:6 or 8:8, is part of the same interaction because all these potentials were computed using the same Cl^- wavefunction. These interactions are presented under separate headings for ready comparison with their 'optimal' counterparts.

For any R less than R'_e, the optimal wavefunction for the 6:6 structure is more contracted than that for $R = R'_e$ so that the overlap between two optimal anion wavefunctions is less than that between the two frozen wavefunctions at the same r_{AA}. The origin of these repulsions in wavefunction overlap suggests that the optimal $V^0_{sAA}(x_{AA}R)$ should, at these $x_{AA}R$, be less repulsive than its frozen counterpart. Similarly, the optimal $V^0_{sAA}(x_{AA}R)$ would be expected to be more repulsive than the frozen one for R greater than R'_e where the optimal wavefunctions being more expanded would overlap more than that used to compute the frozen potential. This behaviour, designated 'normal' [43], is shown in the comparison (table A.1) between the frozen and optimal potentials for the 6:6 phase. Nevertheless, the opposite

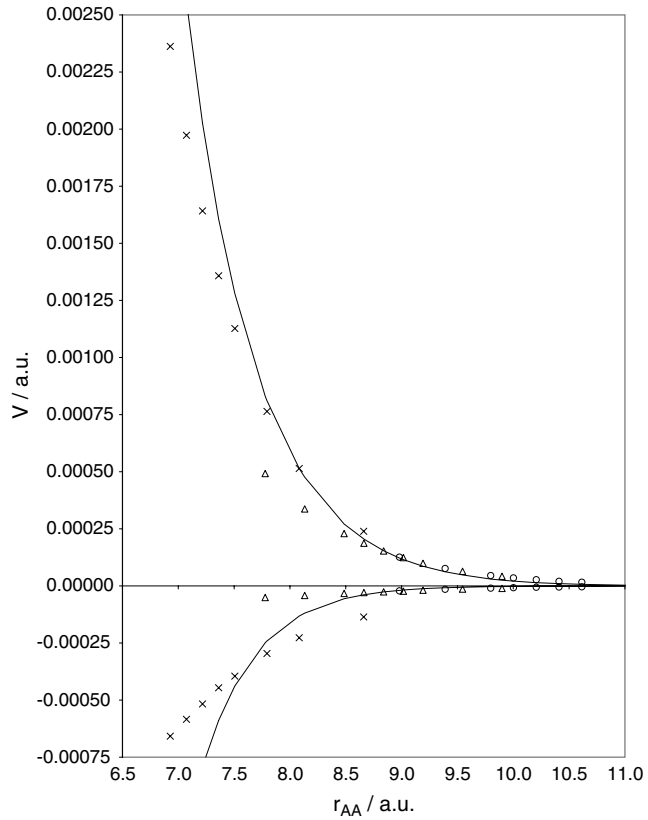

Figure A.1. The permutation $V^0_{\mathrm{AAperm}}(r_{\mathrm{AA}})$ (positive) and penetration $V^0_{\mathrm{AApen}}(r_{\mathrm{AA}})$ (negative) components of the uncorrelated short range anion–anion interaction plotted as a function of anion–anion distance r_{AA}. The solid curves are the frozen potential components with the optimal components denoted by cross (8:8), open triangle (6:6) and open circle (4:4) points. The data for the two smallest r_{AA} for the 8:8 phase are omitted for clarity.

behaviour, with the optimal potential being more repulsive than the frozen one at $R < R'_{\mathrm{e}}$ but becoming less repulsive at larger R, is not uncommon. This behaviour, designated 'mixed', is understood [43] by expressing $V^0_{\mathrm{sAA}}(r_{\mathrm{AA}})$ as the sum of its penetration ($V^0_{\mathrm{AApen}}(r_{\mathrm{AA}})$) and permutation ($V^0_{\mathrm{AAperm}}(r_{\mathrm{AA}})$) components according to

$$V^0_{\mathrm{sAA}}(r_{\mathrm{AA}}) = V^0_{\mathrm{AApen}}(r_{\mathrm{AA}}) + V^0_{\mathrm{AAperm}}(r_{\mathrm{AA}}). \tag{A.1}$$

After subtraction of the point coulomb contribution $q^2_{\mathrm{A}}/r_{\mathrm{AA}}$, where q_{A} is the net charge on ion A, $V^0_{\mathrm{AApen}}(r_{\mathrm{AA}})$ is the interaction energy that would arise, if there was no exchange of electrons between the ions, thus being the residual purely electrostatic interaction energy. $V^0_{\mathrm{AAperm}}(r_{\mathrm{AA}})$ is the sum of all contributions to $V^0_{\mathrm{sAA}}(r_{\mathrm{AA}})$ which arise from interchange of electrons between the ions. The solid lines in figures A.1 and A.2, generated as a smooth curve through the data in table A.1, show how $V^0_{\mathrm{AApen}}(r_{\mathrm{AA}})$ and $V^0_{\mathrm{AAperm}}(r_{\mathrm{AA}})$ vary with r_{AA} for the frozen potential in comparison with the corresponding quantities for the three optimal potentials shown as discreet data points. Contraction of both anions in a pair at constant r_{AA} reduces the overlap of their wavefunctions thus lowering both the repulsive permutation term and the magnitude of the attractive penetration contribution.

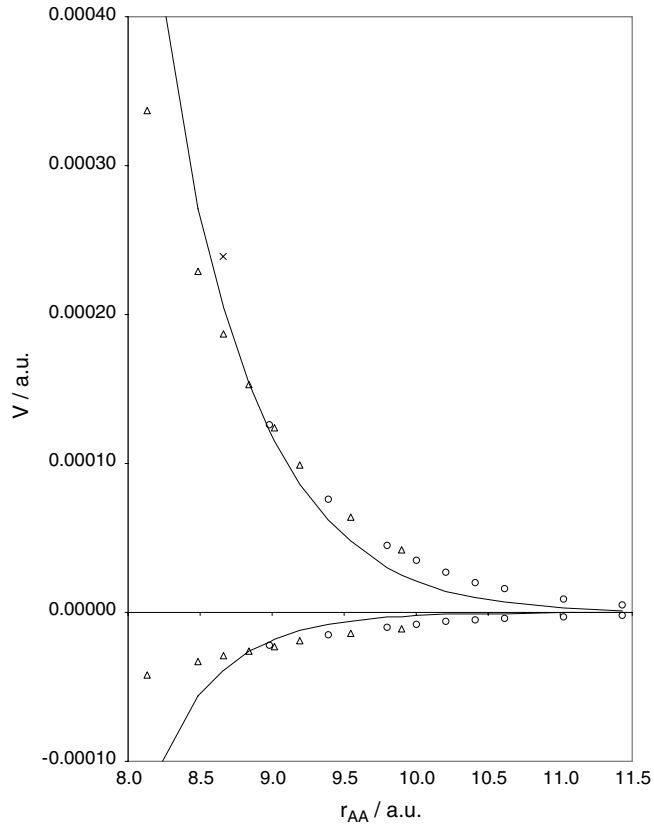

Figure A.2. An expanded presentation of the data of figure A.1 for the larger distances and smaller energies occurring in the 6:6 and 4:4 phases. Data for the 8:8 phase are omitted.

For the 6:6 phase, figures A.1 and A.2 show that both $V^0_{\mathrm{AAperm}}(r_{\mathrm{AA}})$ and the magnitude ($|V^0_{\mathrm{AApen}}(r_{\mathrm{AA}})|$) of the attractive penetration energy for the optimal potential are smaller than those predicted from the frozen potential for $R < R'_{\mathrm{e}}$ (6.25 au), corresponding to an r_{AA} of 8.839 au. This arises because each of the optimal anion wavefunctions is more contracted than that for the R'_{e} used to generate the frozen potential. This situation is reversed for R values greater than R'_{e} where the optimal wavefunctions are more expanded than that used to compute the frozen potential. The comparison of the total $V^0_{\mathrm{sAA}}(r_{\mathrm{AA}})$ potentials shows normal behaviour because, for $R < R'_{\mathrm{e}}$, the lowering of $V^0_{\mathrm{AAperm}}(r_{\mathrm{AA}})$ on passing from the frozen to the optimal potential more than outweighs the reduction of $|V^0_{\mathrm{AApen}}(r_{\mathrm{AA}})|$ with the converse situation occurring for the larger R values. This is shown graphically in the figures because the optimal (open triangle) values for $V^0_{\mathrm{AAperm}}(r_{\mathrm{AA}})$ are further from the corresponding frozen potential (solid curve) than are the optimal values of $V^0_{\mathrm{AApen}}(r_{\mathrm{AA}})$ from their frozen counterparts.

The anion wavefunctions in the 8:8 structure for $R \leqslant 6.25$ au are more contracted than that for the 6:6 phase at R'_{e} as shown (table 2) by their larger rearrangement energies $E^0_{\mathrm{re}}(R)$. For $R = 6.375$ and 6.5 au in the 8:8 phase, $E^0_{\mathrm{re}}(R)$ is also larger than that for 6:6 phase at R'_{e}, showing that the two former wavefunctions are more contracted. These computed results show that the increase in the number of neighbours from 6 to 8 on passing from the 6:6 phase at R'_{e} to the 8:8 phase at $R = 6.375$ au and 6.5 au more than outweighs the increase in R. The

Table A.1. Components of the frozen and optimal OEMFS short range anion–anion potentials (au).

4:4 ($x_{AA} = \sqrt{(8/3)}$)							
	$V^0_{pen}(\sqrt{8}R/\sqrt{3})$		$V^0_{perm}(\sqrt{8}R/\sqrt{3})$		$V^0_S(\sqrt{8}R/\sqrt{3})$		$V_S(\sqrt{8}R/\sqrt{3})$
R	Frozen	Optimal	Frozen	Optimal	Frozen	Optimal	Frozen
5.5	−0.000 020	−0.000 022	0.000 122	0.000 126	0.000 103	0.000 104	0.000 006
5.75	−0.000 008	−0.000 015	0.000 062	0.000 076	0.000 054	0.000 061	−0.000 001
6.0	−0.000 003	−0.000 010	0.000 030	0.000 045	0.000 027	0.000 036	−0.000 003
6.125	−0.000 002	−0.000 008	0.000 021	0.000 035	0.000 019	0.000 027	−0.000 003
6.25	−0.000 001	−0.000 006	0.000 014	0.000 027	0.000 013	0.000 021	−0.000 003
6.375	−0.000 001	−0.000 005	0.000 010	0.000 020	0.000 009	0.000 016	−0.000 002
6.5	−0.000 001	−0.000 004	0.000 007	0.000 016	0.000 006	0.000 012	−0.000 002
6.75	0.0	−0.000 003	0.000 003	0.000 009	0.000 003	0.000 007	−0.000 001
7.0	0.0	−0.000 002	0.000 001	0.000 005	0.000 001	0.000 004	−0.000 001
6:6 ($x_{AA} = \sqrt{2}$)							
	$V^0_{pen}(\sqrt{2}R)$		$V^0_{perm}(\sqrt{2}R)$		$V^0_S(\sqrt{2}R)$		$V_S(\sqrt{2}R)$
R	Frozen	Optimal	Frozen	Optimal	Frozen	Optimal	Frozen
5.5	−0.000 249	−0.000 051	0.000 831	0.000 492	0.000 582	0.000 441	0.000 176
5.75	−0.000 119	−0.000 042	0.000 476	0.000 337	0.000 357	0.000 296	0.000 082
6.0	−0.000 056	−0.000 033	0.000 271	0.000 229	0.000 215	0.000 196	0.000 034
6.125	−0.000 039	−0.000 029	0.000 205	0.000 187	0.000 166	0.000 158	0.000 020
6.25	−0.000 026	−0.000 026	0.000 154	0.000 153	0.000 128	0.000 127	0.000 011
6.375	−0.000 018	−0.000 023	0.000 115	0.000 124	0.000 097	0.000 101	0.000 004
6.5	−0.000 012	−0.000 019	0.000 086	0.000 099	0.000 074	0.000 080	0.000 001
6.75	−0.000 006	−0.000 014	0.000 048	0.000 064	0.000 042	0.000 050	−0.000 002
7.0	−0.000 003	−0.000 011	0.000 025	0.000 042	0.000 022	0.000 031	−0.000 003
8:8 ($x_{AA} = [2/\sqrt{3}]$)							
	$V^0_{pen}(2R/\sqrt{3})$		$V^0_{perm}(2R/\sqrt{3})$		$V^0_S(2R/\sqrt{3})$		$V_S(2R/\sqrt{3})$
R	Frozen	Optimal	Frozen	Optimal	Frozen	Optimal	Frozen
5.5	−0.004 430	−0.001 147	0.008 496	0.004 936	0.004 066	0.003 789	0.002 380
5.75	−0.002 514	−0.000 857	0.005 211	0.003 403	0.002 697	0.002 547	0.001 411
6.0	−0.001 415	−0.000 658	0.003 233	0.002 362	0.001 818	0.001 704	0.000 845
6.125	−0.001 058	−0.000 584	0.002 558	0.001 973	0.001 499	0.001 389	0.000 655
6.25	−0.000 790	−0.000 517	0.002 026	0.001 642	0.001 236	0.001 126	0.000 505
6.375	−0.000 589	−0.000 446	0.001 606	0.001 358	0.001 018	0.000 912	0.000 387
6.5	−0.000 438	−0.000 395	0.001 280	0.001 127	0.000 842	0.000 732	0.000 299
6.75	−0.000 241	−0.000 296	0.000 811	0.000 764	0.000 570	0.000 468	0.000 171
7.0	−0.000 132	−0.000 227	0.000 514	0.000 514	0.000 383	0.000 287	0.000 092
7.5	−0.000 039	−0.000 136	0.000 206	0.000 239	0.000 167	0.000 103	0.000 020

greater contraction of all these 8:8 anion wavefunctions explains why the optimal $V^0_{AAperm}(r_{AA})$ and $|V^0_{AApen}(r_{AA})|$ are smaller than their frozen counterparts (figure A.1). The comparison between the optimal and frozen V^0_{sAA} (r_{AA}) shows normal behaviour because (figure A.1) the optimal (cross) $V^0_{AAperm}(r_{AA})$ values lie further from the frozen potential results than do optimal $V^0_{AApen}(r_{AA})$ from their frozen counterparts. For $R = 7.5$ au, the optimal anion wavefunction

in the 8:8 structure is more expanded than the 6:6 function for $R = R'_e$ as shown by the smaller $E^0_{re}(R)$ of the former (table 2). This explains why the optimal $V^0_{AAperm}(r_{AA})$ and $|V^0_{AApen}(r_{AA})|$ are larger than their frozen counterparts. However, the comparison of the optimal and frozen $V^0_{sAA}(r_{AA})$ shows mixed behaviour with the optimal potential being smaller because the increase in the repulsive $V^0_{AAperm}(x_{AA}R)$ on passing from the frozen to the optimal wavefunction is less than the increase of $|V^0_{AApen}(x_{AA}R)|$ as shown in figure A.1. The $E^0_{re}(R)$ in table 2 show that for $R > 5.5$ au the anion wavefunctions in the 4:4 structure are expanded relative to that for the 6:6 phase at $R = R'_e$. This has the consequence (figure A.2) that these optimal $V^0_{AAperm}(r_{AA})$ and $|V^0_{AApen}(r_{AA})|$ are greater than their frozen counterparts. The comparison, when passing from the frozen to the optimal total potentials, shows normal behaviour because the increase in $V^0_{AAperm}(r_{AA})$ is greater than that of $|V^0_{AApen}(r_{AA})|$.

In the 6:6 and 8:8 phases, for each of the three pairs of R values (5.5, 6.75), (5.75, 7.0) and (6.125, 7.5) listing the 6:6 distance first, the r_{AA} are essentially the same (figure A.1) on account of different factors x_{AA}. Comparison of the two $E^0_{re}(R)$ in each of the three pairs shows the wavefunction in the 6:6 phase to be more compressed. This explains why $V^0_{AAperm}(x_{AA}R)$ and $|V^0_{AApen}(x_{AA}R)|$ are smaller (figure A.1) for the 6:6 phase in each pair. Although comparison of the two potentials in the first pair shows normal behaviour with $V^0_{sAA}(r_{AA})$ for the 8:8 structure being greater than that in the 6:6 phase, comparison of the potentials in both the latter pairs shows mixed behaviour, the repulsion being greater in the 6:6 phase, as was previously reported for MgO [43].

References

[1] Pyper N C 1991 *Adv. Solid State Chem.* **2** 223
[2] Madden P A and Wilson M 1996 *Chem. Soc. Rev.* **25** 339
[3] Mansikka K 1961 *Ann. Acad. Sci. Fenn.* A **6** 81
[4] Jarvinen M and Inkinen O 1967 *Phys. Status Solidi* **21** 127
[5] Pyper N C 1986 *Phil. Trans. R. Soc.* A **320** 107
[6] Pyper N C 1994 *Chem. Phys. Lett.* **220** 70
[7] Pyper N C 1995 *Phil. Trans. R. Soc.* A **352** 89
[8] Harding J H, Lindan P J D and Pyper N C 1994 *J. Phys.: Condens. Matter* **6** 6485
[9] Pyper N C and Popelier P 1995 *J. Phys.: Condens. Matter* **7** 5013
[10] Pyper N C 1995 *J. Phys.: Condens. Matter* **7** 9127
[11] Pyper N C 1996 *J. Phys.: Condens. Matter* **8** 5509
[12] Pyper N C 2003 *J. Chem. Phys.* **118** 2308
[13] Hund F 1925 *Z. Phys.* **34** 833
[14] May A 1937 *Phys. Rev.* **52** 339
[15] May A 1938 *Phys. Rev.* **54** 629
[16] Tosi M P and Fumi F G 1962 *J. Phys. Chem. Solids* **23** 359
[17] Goldschmidt V M, Barth T, Lunde G and Zachariasen W H 1926 *Skr. Nor. Vidensk.-Akad. Oslo* **1** 1
[18] Pauling L 1927 *J. Am. Chem. Soc.* **49** 756
[19] Wells A F 1962 *Structural Inorganic Chemistry* (Oxford: Oxford University Press)
[20] Ladd M F C 1968 *Theor. Chim. Acta* **12** 333
[21] Gouray B S and Adrian F J 1960 *Solid State Physics: Advances in Research and Applications* vol 10, ed F Seitz and D Turnbull (New York: Wiley) p 128
[22] Morris D F C 1968 *Struct. Bond.* **4** 63
[23] Wagner G and Lippert L 1936 *Z. Phys. Chem.* B **31** 297
[24] Blackman M and Kahn I H 1961 *Proc. Phys. Soc.* **77** 471
[25] Ostwald W 1897 *Z. Phys. Chem.* **22** 289
[26] Stranski I N and Totomanow D 1933 *Z. Phys. Chem.* **163** 399
[27] Meyer R R, Sloan J, Dunin-Borkowski R E, Kirkland A I, Novotny M C, Bailey S R, Hutchinson J L and Green M L H 2000 *Science* **289** 1324

[28] Sloan J, Novotny M C, Bailey S R, Brown G, Xu C, Williams V C, Friedrichs S, Flahaut E, Callender R L, York A P E, Coleman K S, Green M L H, Dunin-Borkowski R E and Hutchinson J L 2000 *Chem. Phys. Lett.* **329** 61
[29] Sloan J, Kirkland A I, Hutchison J L and Green M L H 2002 *Chem. Commun.* 1319
[30] Sloan J, Friedrichs S, Meyer R R, Kirkland A I, Hutchison J L and Green M L H 2002 *Inorg. Chim. Acta* **330** 1
[31] Sloan J, Kirkland A I, Hutchison J L and Green M L H 2003 *Comptes Rendu* **4** 1063
[32] Kirkland A I, Saxton W O and Chand G 1997 *J. Electron Microsc.* **46** 11
[33] Meyer R R, Kirkland A I and Saxton W O 2002 *Ultramicroscopy* **92** 89
[34] Philp E, Sloan J, Kirkland A I, Meyer R R, Friedrichs S, Hutchison J L and Green M L H 2003 *Nat. Mater.* **2** 778
[35] Wilson M and Madden P A 2001 *J. Am. Chem. Soc.* **123** 2101
[36] Wilson M 2002 *J. Chem. Phys.* **116** 3027
[37] Pyper N C 1990 *Mol. Simul.* **5** 23
[38] Abarenkov I V and Antonova I M 1970 *Phys. Status Solidi* **38** 783
[39] Wood C P and Pyper N C 1981 *Chem. Phys. Lett.* **81** 395
[40] Wood C P and Pyper N C 1986 *Phil. Trans. R. Soc.* A **320** 71
[41] Grant I P, McKenzie B J, Norrington P H, Mayers D F and Pyper N C 1980 *Comput. Phys. Commun.* **21** 207
[42] Pyper N C and Harding J H 2005 in preparation
[43] Pyper N C 2001 *J. Chem. Phys.* **114** 4390
[44] Marks N A, Finnis M W, Harding J H and Pyper N C 2001 *J. Chem. Phys.* **114** 4406
[45] Wilson M, Madden P A, Pyper N C and Harding J H 1996 *J. Chem. Phys.* **104** 8068
[46] Fowler P W and Pyper N C 1985 *Proc. R. Soc.* A **398** 377
[47] Fowler P W, Knowles P J and Pyper N C 1985 *Mol. Phys.* **56** 83
[48] Wilson J N and Curtiss R M 1970 *J. Phys. Chem.* **74** 187
[49] Pyper N C and Popelier P 1997 *J. Phys.: Condens. Matter* **9** 471
[50] Landolt-Bornstein Z 1966 *Series III* vol 1 (Berlin: Springer)
[51] Cortona P 1992 *Phys. Rev.* B **46** 2008
[52] Rae A I M 1973 *Chem. Phys. Lett.* **18** 574
[53] Rae A I M 1975 *Mol. Phys.* **29** 467
[54] Wood C P and Pyper N C 1981 *Mol. Phys.* **43** 1371
[55] Lacks D J and Gordon R G 1993 *Phys. Rev.* A **47** 4681
[56] Cohen A J and Gordon R G 1975 *Phys. Rev.* B **12** 3228
[57] Gordon R G and Kim Y S 1972 *J. Chem. Phys.* **56** 3122
[58] Muhlhausen C and Gordon R G 1981 *Phys. Rev.* B **23** 900
[59] Waldman M and Gordon R G 1979 *J. Chem. Phys.* **71** 1325
[60] Waldman M and Gordon R G 1979 *J. Chem. Phys.* **71** 1340
[61] Mei W N, Boyer L L, Mehl M J, Ossowski M M and Stokes H T 2000 *Phys. Rev.* B **61** 11425
[62] Gale J D 1997 *J. Chem. Soc. Faraday Trans.* **93** 629
[63] Simons G, Parr R G and Finlan J M 1973 *J. Chem. Phys.* **59** 3229
[64] Weast R C (ed) 2003 *CRC Handbook of Chemistry and Physics* 84th edn (Boca Raton, FL: CRC Press)
[65] Sangser M J L, Schroder U and Atwood R M 1978 *J. Phys. C: Solid State Phys.* **11** 1523
[66] Harding J H 1985 *Phys. Rev.* B **32** 6861
[67] Weast R C (ed) 1979 *CRC Handbook of Chemistry and Physics* 59th edn (Boca Raton, FL: CRC Press)
[68] Gray D E (ed) 1973 *AIP Handbook* (New York: McGraw-Hill)
[69] Weast R C (ed) 1994 *CRC Handbook of Chemistry and Physics* 75th edn (Boca Raton, FL: CRC Press)
[70] Lewis J T, Lehoczky A and Briscoe C V 1967 *Phys. Rev.* **161** 877